J Solid State Electrochem (2007) 11: 117–125
DOI 10.1007/s10008-005-0080-0

ORIGINAL PAPER

**Ju-Sik Kim · Su-Il Pyun · Jong-Won Lee · Rak-Hyun Song**

# Kinetics of oxygen reduction on porous mixed conducting $(La_{0.85}Sr_{0.15})_{0.9}MnO_3$ electrode by ac-impedance analysis

Received: 21 July 2005 / Revised: 21 October 2005 / Accepted: 9 November 2005 / Published online: 3 January 2006


**Abstract** The oxygen reduction reaction on mixed conducting $(La_{0.85}Sr_{0.15})_{0.9}MnO_3$ electrodes with various porosities was investigated by analysis of the ac-impedance spectra. To attain a mixed electronic/ionic conducting state of $(La_{0.85}Sr_{0.15})_{0.9}MnO_3$ with high oxygen vacancy concentration, the electrode specimen was purposely subjected to cathodic polarisation. The ac-impedance spectrum clearly showed a straight line inclined at a constant angle of 45° to the real axis in the high-frequency range, followed by an arc in the low-frequency range, i.e. it exhibited the Gerischer behaviour. This strongly indicates that oxygen reduction on the mixed conducting electrode involves diffusion of oxygen vacancy through the electrode coupled with the electron exchange reaction between oxygen vacancies and gaseous oxygen (charge transfer reaction) at the electrode/gas interface. It was further recognised that the two-dimensional electrochemical active region for oxygen reduction extends from the origin of the three-phase boundaries (TPBs) among electrode, electrolyte and gas into the electrode/gas interface segments, which is on average approximately 0.7 to 1.1 μm in length below the electrode porosity 0.12. Based from the fact that the ac-impedance spectrum deviated more significantly from the Gerischer behaviour with increasing electrode porosity above 0.22, it is proposed that due to the increased length of TPBs, the rate of the overall oxygen reduction on the highly porous electrode is mainly determined by the charge transfer reaction at the TPBs, and the subsequent diffusion of oxygen vacancy occurs facilely through the electrode.

J.-S. Kim · S.-I. Pyun (✉) · J.-W. Lee
Department of Materials Science and Engineering,
Korea Advanced Institute of Science and Technology,
373-1 Guseong-Dong, Yuseong-Gu,
Daejeon 305-701, Republic of Korea
e-mail: sipyun@webmail.kaist.ac.kr
Tel.: +82-42-8693319
Fax: +82-42-8693310

R.-H. Song
Korea Institute of Energy Research,
71-2 Jang-Dong, Yuseong-Gu,
Daejeon 305-343, Republic of Korea

**Keywords** Solid oxide fuel cell · $(La_{0.85}Sr_{0.15})_{0.9}MnO_3$ · Mixed electronic/ionic conductor · Oxygen reduction · Ac-impedance spectroscopy

## Introduction

In recent years, the environmental friendly solid oxide fuel cell (SOFC) has been considered as one of the most efficient power generation systems [1, 2]. Especially, due to its high operating temperatures, the SOFC offers several potential advantages over polymer-based fuel cells, including fast electrode kinetics, high tolerance to typical catalyst poisons, internal reforming and direct use of hydrocarbon fuels [2, 3]. Among various kinds of oxide materials, strontium-doped lanthanum manganite, i.e. $(La_{1-x}Sr_x)_{1-y}MnO_3$ ($x$=0.05 to 0.4 and $y$=0 to 0.1), has been widely used as a cathode material for the SOFC, owing to its high electrocatalytic activity for oxygen reduction, high electrical conductivity and good chemical/thermal compatibilities with zirconia electrolytes [3, 4].

During the SOFC operation, the overpotential is mainly given by the cathodic oxygen reduction reaction [5]. In this respect, the mechanism of oxygen reduction on the $(La_{1-x}Sr_x)_{1-y}MnO_3$ electrode has been extensively investigated by employing ac-impedance spectroscopy [6–15], which provides an exceptionally powerful tool for separating the dynamics of several electrode processes with different relaxation times.

In contrast to the strontium-doped $LaCoO_3$ with a mixed electronic/ionic conducting property, the $(La_{1-x}Sr_x)_{1-y}MnO_3$ electrode predominantly shows an electronic conducting behaviour, since the substitution of $Sr^{2+}$ for $La^{3+}$ increases the $Mn^{4+}$ content in the electrode rather than the concentration of oxygen vacancies [16]. Therefore, most researchers [6–8, 12–15] have interpreted their ac-impedance spectra measured on the $(La_{1-x}Sr_x)_{1-y}MnO_3$ electrode under the assumption that only the three-phase boundaries (TPBs) among electrode, electrolyte and gas provide the electrochemical active sites for the oxygen reduction reaction.

However, it has been reported [17, 18] that the $(La_{1-x}Sr_x)_{1-y}MnO_3$ electrode subjected to a large cathodic polarisation undergoes the partial reduction of $Mn^{3+}$ to $Mn^{2+}$, leading to the formation of oxygen vacancies in the electrode itself. This indicates that during the SOFC operation the electrode can be so altered that it has a mixed conducting property. Nevertheless, relatively little attention has been paid to the oxygen reduction reaction on the mixed conducting $(La_{1-x}Sr_x)_{1-y}MnO_3$ electrode with high oxygen vacancy concentration.

The present work considers the oxygen reduction reaction on the porous mixed conducting $(La_{0.85}Sr_{0.15})_{0.9}MnO_3$ electrode by using ac-impedance spectroscopy. Firstly, to attain a mixed conducting state of $(La_{0.85}Sr_{0.15})_{0.9}MnO_3$, the electrode was purposely subjected to cathodic polarisation. Secondly, the ac-impedance spectra measured at various temperatures and oxygen partial pressures were quantitatively analysed by employing the theoretical impedance model developed by Adler et al. [19] for oxygen reduction on the mixed conducting electrode. Finally, the influences of the electrode porosity on the oxygen reduction kinetics were discussed based upon the measured impedance spectra.

## Experimental

### Preparation of $(La_{0.85}Sr_{0.15})_{0.9}MnO_3$ specimen

The $(La_{0.85}Sr_{0.15})_{0.9}MnO_3$ powder was prepared by calcinating a pressed mixture of $La_2O_3$ (Aldrich, USA, purity 99.9%), $MnO_2$ (Aldrich, purity 98.0%) and $SrCO_3$ (Aldrich, purity 99.9%) at 1,273 K for 5 h in air with intermittent grindings. The resulting powder specimen was further ground to below 1 μm in particle size by ball milling. To identify the crystal structure of the $(La_{0.85}Sr_{0.15})_{0.9}MnO_3$ powder, x-ray diffraction (XRD) patterns were recorded on an automated Rigaku diffractometer (Rigaku, D/max-RC) using Cu Kα radiation. Figure 1 shows the XRD pattern of the $(La_{0.85}Sr_{0.15})_{0.9}$ $MnO_3$ powder. In the XRD analysis, it was found that the $(La_{0.85}Sr_{0.15})_{0.9}MnO_3$ powder showed the well-known perovskite structure.

The slurries with various viscosities were made by mixing the $(La_{0.85}Sr_{0.15})_{0.9}MnO_3$ powder with 5 to 52 wt.% polyvinyl butyral ($CH_2$–1,2–$[(CH)_3CH_2O_2C_3H_7]$) binder in toluene ($C_6H_5CH_3$) and 2-propanol ($(CH_3)_2CHOH$). Moreover, 2.5 wt.% dibutyl phthalate ($C_6H_4$–1,2–$[CO_2(CH_2)_3CH_3]_2$) (plasticiser), 1.4 wt.% Triton-X (homogeniser) and 3.0 wt.% fish oil (dispersant) were added to the slurry.

### Preparation of three-electrode electrochemical cell

In this work, 8 mol% $Y_2O_3$-stabilised $ZrO_2$ (YSZ) squared pellet 1.0 cm×1.1 cm×0.2 mm in size (Tosoh Co., Japan) was used as the electrolyte. The $(La_{0.85}Sr_{0.15})_{0.9}MnO_3$ slurry was first coated on one side of the YSZ pellet using the screen printing method, followed by sintering at

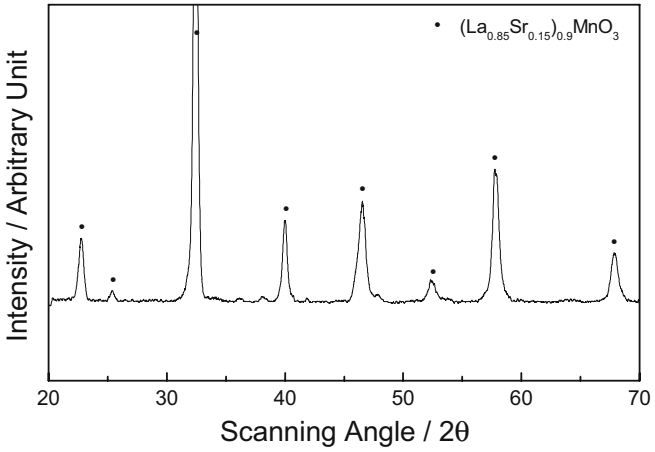


**Fig. 1** XRD patterns of the $(La_{0.85}Sr_{0.15})_{0.9}MnO_3$ powder that was prepared by calcinating a pressed mixture of $La_2O_3$, $MnO_2$ and $SrCO_3$ at 1,273 K for 5 h in air with intermittent grindings

1,623 K for 30 min in air. The counter and reference electrodes were then prepared by printing Pt pastes on the other side of the YSZ pellet, respectively, followed by firing at 1,273 K for 1 h in air. The reference electrode was 4 mm away from the counter electrode to circumvent the difficulties in potential distortion in the bulk electrolyte. The working, counter and reference electrodes were coated over areas 0.6, 0.8 and 0.2 $cm^2$, respectively. To provide electrical conduction, Pt meshes and wires were finally attached onto the three kinds of the electrodes with Pt paste and fired at 1,223 K for 30 min in air. The schematic diagram of the cell configuration employed in the present work is given in Fig. 2.

### Electrochemical measurements

For the purpose of investigating the electrochemical behaviour of the mixed conducting $(La_{0.85}Sr_{0.15})_{0.9}MnO_3$ electrode, the as-sintered electrode was previously subjected to the cathodic polarisation of −0.9 V at 1,273 K for

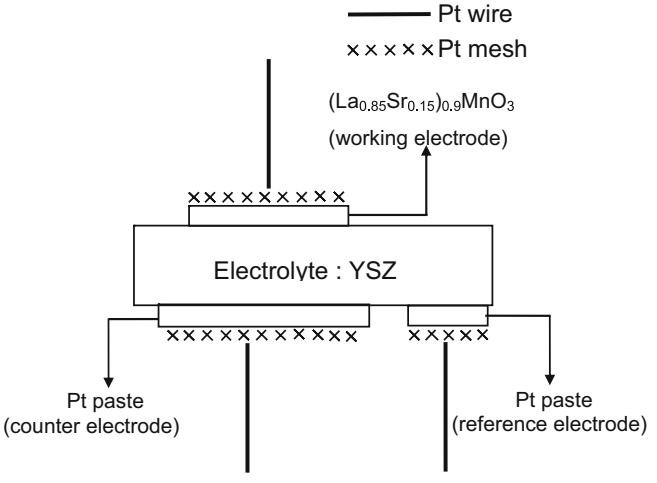


**Fig. 2** Schematic diagram of the cell configuration employed for the ac-impedance measurement

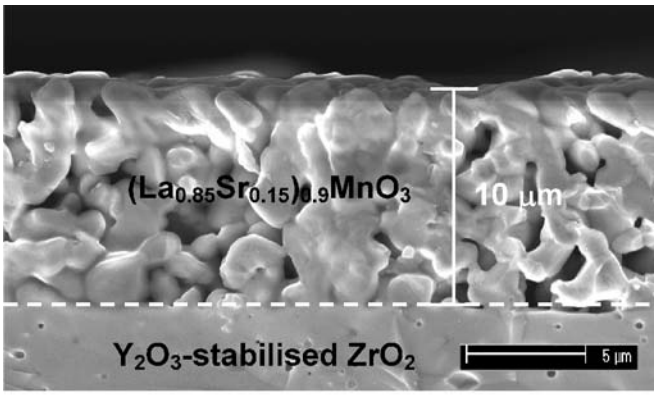


a

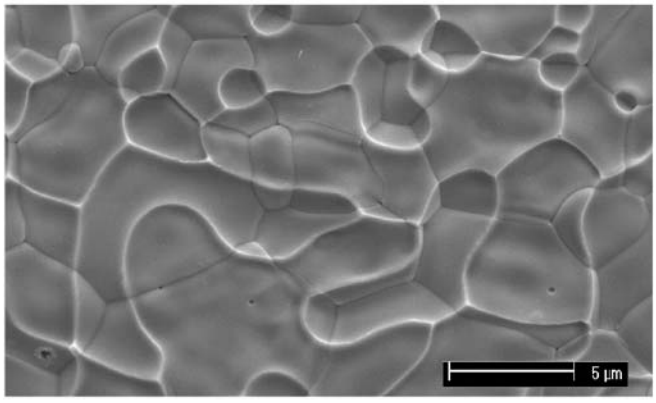


b

**Fig. 3** SEM micrographs of the cross-section of the $(La_{0.85}Sr_{0.15})_{0.9}MnO_3$ electrode coated on the 8 mol% $Y_2O_3$-stabilised $ZrO_2$ (YSZ) pellet from the slurry with 52 wt.% polyvinyl butyral binder **a** and the YSZ surface obtained after dissolving the $(La_{0.85}Sr_{0.15})_{0.9}MnO_3$ electrode in 1 mol HCl solution **b**

6 h in air by using a Solartron 1,287 electrochemical interface (ECI). Ac-impedance measurement was then performed with a Solartron 1,255 frequency response analyser combined with a Solartron 1,287 ECI. Ac-impedance spectra were measured on the $(La_{0.85}Sr_{0.15})_{0.9}MnO_3$ electrode at the open circuit potential by applying an ac-amplitude of 5 $mV_{rms}$ over the frequency range from $10^{-2}$ to $10^5$ Hz in atmospheres of the $O_2/N_2$ gas mixtures with the oxygen partial pressures $p_{O_2}$ 0.04 to 0.21 atm at various temperatures $T$ ranging from 1,123 to 1,273 K.

## Results and discussion

### Characterisation of the porous $(La_{0.85}Sr_{0.15})_{0.9}MnO_3$ electrode

Figure 3a gives the typical scanning electron microscopic (SEM) image of the cross-section of the $(La_{0.85}Sr_{0.15})_{0.9}MnO_3$ electrode coated on the YSZ pellet from the slurry with 52 wt.% polyvinyl butyral binder. The coated $(La_{0.85}Sr_{0.15})_{0.9}MnO_3$ electrode had a porous structure, and its thickness was estimated to be about 10 μm. In the simple comparison of the pore geometry shown in Fig. 3a with the reference pore geometries typically reported in the literature [20], the pore tortuosity $\tau$ of the $(La_{0.85}Sr_{0.15})_{0.9}MnO_3$ electrode was roughly estimated to be 2.5. The surface area $A_s$ of the porous $(La_{0.85}Sr_{0.15})_{0.9}MnO_3$ electrode per unit volume was calculated under the assumption that $A_s$ is identical to the total surface area of the electrode composed of the spherical particles from the calculated $\varepsilon$ and the mean particle size measured from the SEM image in Fig. 3a.

Figure 3b presents the SEM image obtained from the YSZ surface after dissolving the porous $(La_{0.85}Sr_{0.15})_{0.9}MnO_3$ layer in 1 mol HCl solution for 5 min. The lines that look bright are considered to be the TPBs among electrode, electrolyte and gas. The SEM picture of Fig. 3b was digitised with an image scanner, and then it was transformed to a binary image to quantitatively evaluate the length of TPBs $l_{TPB}$ and the contact area $A_{cont}$ between the electrode and the electrolyte. Here, the image was transformed to its brightness on a scale from 0 to 255, and subsequently any brightness larger and smaller than 130 were set at 0 and 255, respectively.

The electrode porosity $\varepsilon$ [21] was merely calculated from the measured value of $A_{cont}$ from

$$\varepsilon = 1 - \frac{A_{cont}}{A_g} \quad (1)$$

where $A_g$ is the geometric area of the electrode. The values of $\varepsilon$ obtained from Eq. (1) were quite well consistent with those values evaluated from the comparison of the theoretical density (6.55 g $cm^{-3}$; [21]) and apparent density. The apparent density was measured using the mass and thickness of the electrode from Fig. 3a. Table 1 lists all the geometric parameters mentioned above which

**Table 1** Geometric parameters of the porous $(La_{0.85}Sr_{0.15})_{0.9}MnO_3$ electrodes coated on the YSZ electrolyte from the slurries with various contents of polyvinyl butyral binder

| Binder content in the slurry (wt.%) | Apparent density, $\rho_A$ (g $cm^{-3}$) | Tortuosity, $\tau$ (–) | Surface area per unit volume, $A_s$ ($\mu m^{-1}$) | TPB length per unit area, $l_{TPB}$[a] ($\mu m^{-1}$) | Contact area, $A_{cont}$ ($\mu m^2$) | Porosity, $\varepsilon$ (–) |
|---|---|---|---|---|---|---|
| 5 | 4.28 | 2.5 | 1.8 | 0.57 | $4.0\times10^7$ | 0.33 |
| 30 | 5.26 | 2.5 | 1.32 | 0.51 | $4.6\times10^7$ | 0.22 |
| 0.53 | 5.81 | 2.5 | 0.95 | 0.45 | $5.2\times10^7$ | 0.12 |

[a] $l_{TPB}$ means number of the active reaction sites per unit TPB length

were determined from the porous $(La_{0.85}Sr_{0.15})_{0.9}MnO_3$ electrodes coated on the YSZ electrolyte from the slurries with various contents of polyvinyl butyral binder.

## Ac-impedance behaviour of the as-sintered $(La_{0.85}Sr_{0.15})_{0.9}MnO_3$ electrode

It is generally accepted [22, 23] that the $(La_{0.85}Sr_{0.15})_{0.9}MnO_3$ electrode is a predominantly electronic conductor, rather than a mixed conductor, hence only the TPBs provide the electrochemical active region for oxygen reduction. In this case, the oxygen reduction reaction is known to proceed through four consecutive steps [6–8, 10–15]: (i) diffusion of gaseous oxygen through the pores in the electrode, (ii) adsorption of oxygen molecule on the electrode surface, (iii) diffusion of adsorbed oxygen atom along the electrode surface towards the TPBs and (iv) the charge transfer reaction at the TPBs.

Figure 4a,b demonstrate the Nyquist plots of the ac-impedance spectrum obtained from the as-sintered $(La_{0.85}Sr_{0.15})_{0.9}MnO_3$ electrode with $\varepsilon = 0.12$ as a function of $T$ at $p_{O_2}$ =0.04 atm and as a function of $p_{O_2}$ at $T$=1,273 K, respectively. All the measured impedance spectra simply consisted of two depressed arcs which overlapped slightly over the whole $T$ and $p_{O_2}$ ranges. It is also shown in Fig. 4a,b that the magnitude of the high-frequency arc decreased significantly with increasing $T$, but it remained nearly constant regardless of $p_{O_2}$. In contrast, the low-frequency arc remained almost unchanged in magnitude irrespective of the value of $T$, while it was highly dependent on the value of $p_{O_2}$.

In general, it has been reported [12, 13, 15] that both the diffusion reaction of gaseous oxygen through the pores and the adsorption reaction of oxygen molecule on the electrode surface are too facile to affect oxygen reduction at $T$>1,173 K and $p_{O_2}$ >0.01 atm. From the experimental results that the magnitudes of the high- and low-frequency arcs strongly depend on the values of $T$ and $p_{O_2}$ as shown in Fig. 4a,b, respectively, it is thus deduced that the high-frequency arc is attributed to the charge transfer reaction at the TPBs, and the low-frequency arc is associated with diffusion of adsorbed oxygen atom along the electrode/gas interface.

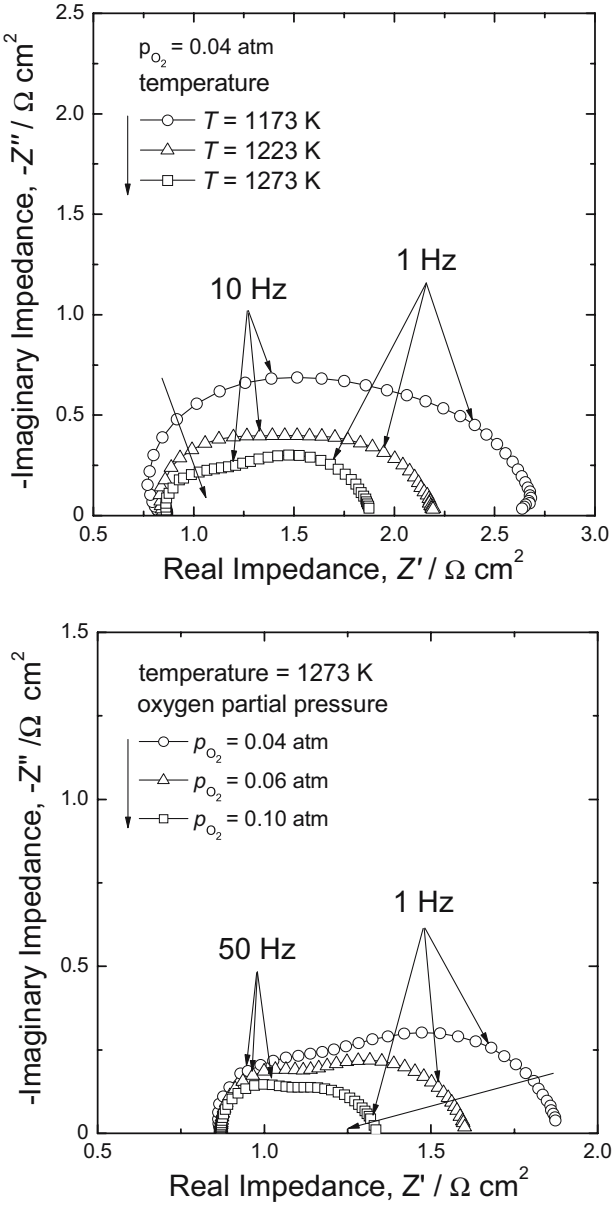


**Fig. 4** Nyquist plots of the ac-impedance spectrum measured on the as-sintered $(La_{0.85}Sr_{0.15})_{0.9}MnO_3$ electrode with $\varepsilon$=0.12: **a** obtained as a function of $T$ at $p_{O_2}$=0.04 atm; **b** obtained as a function of $p_{O_2}$ at $T$=1,273 K

## Theoretical consideration

Now, we consider some basic aspects of the theoretical impedance model for oxygen reduction on the porous mixed electronic/ionic conductor developed by Adler et al. [19]. Let us assume that the overall oxygen reduction reaction on the mixed conducting electrode is split into the following two consecutive substeps: diffusion of oxygen vacancy through the electrode and subsequent electron exchange reaction between oxygen vacancies and gaseous oxygen (charge transfer reaction) at the electrode/gas interface. For simplicity, we leave the diffusion reactions of gaseous oxygen through the pores and of adsorbed oxygen atom along the electrode/gas interface out of consideration.

The governing equation for oxygen vacancy transport through the electrode is given as the modified Fick's diffusion equation as follows [19]:

$$(1-\varepsilon)\frac{\partial(\delta c_{V_O^{\cdot\cdot}})}{\partial t} = \left(\frac{1-\varepsilon}{\tau}\right) W_{th} D_{V_O^{\cdot\cdot}} \frac{\partial^2(\delta c_{V_O^{\cdot\cdot}})}{\partial y^2} - A_s j_{int} \qquad (2)$$

with the instantaneous exchange flux $j_{int}$ at the electrode/gas interface,

$$j_{int} = j_o\left\{\exp\left(\frac{\alpha_1}{RT}\Delta\mu_{int}\right) - \exp\left(-\frac{(1-\alpha_1)}{RT}\Delta\mu_{int}\right)\right\} \quad (3)$$

where $c_{V_o^{\cdot\cdot}}$ is the oxygen vacancy concentration in the electrode, $\delta c_{V_o^{\cdot\cdot}}$ the deviation of $c_{V_o^{\cdot\cdot}}$ from the initial concentration, $t$ the diffusion time of oxygen vacancy, $W_{th}$ the thermodynamic enhancement factor of the component diffusivity of oxygen vacancy, $D_{V_o^{\cdot\cdot}}$ the component diffusivity of oxygen vacancy, $y$ the distance from the electrode/electrolyte interface towards the bulk electrode, $j_o$ the equilibrium exchange flux at $t=\infty$, $\alpha_1$ the transfer coefficient for oxygen absorption, $\Delta\mu_{int}$ the difference between the chemical potentials of oxygen vacancies in the electrode and gaseous oxygen, and $R$ represents the gas constant.

Solving the modified Fick's diffusion equation of Eq. (2) under the boundary conditions of the oscillating concentration (or potential) perturbation at the electrode/electrolyte interface ($y=0$) and of the semi-infinite diffusion of oxygen vacancy, the following expression for $\delta c_{V_o^{\cdot\cdot}}$ is obtained [19]:

$$\delta c_{V_o^{\cdot\cdot}} = \frac{E_o F c_{V_o^{\cdot\cdot}}}{W_{th}RT}\exp\left(-\frac{y}{\lambda}\sqrt{1-j\omega t_{ch}} - j\omega t_{ch}\right) \quad (4)$$

$$\text{with } t_{ch} = \frac{c_{V_o^{\cdot\cdot}}(1-\varepsilon)}{W_{th}A_s j_o} \quad (5)$$

$$\text{and } \lambda = \sqrt{\frac{c_{V_o^{\cdot\cdot}}D_{V_o^{\cdot\cdot}}(1-\varepsilon)}{\tau A_s j_o}} \quad (6)$$

where $E_o$ is the ac-amplitude of the oscillating potential, $\omega$ is the angular frequency, $j$ is the unit of the complex number $\left(\sqrt{-1}\right)$ and $t_{ch}$ denotes in a first approximation the characteristic time constant required for diffusion of oxygen vacancy from the electrode/gas interface through the electrode to the electrode/electrolyte interface. In addition, $\lambda$ represents the distance at which the value of $\delta c_{V_o^{\cdot\cdot}}$ drops to $(1/e)$ of the value at $y=0$ at steady-state ($\omega=0$).

The electric current $I$ [A] at the electrode/electrolyte interface is expressed by

$$I = -\frac{2F(1-\varepsilon)}{\tau}W_{th}D_{V_o^{\cdot\cdot}}\frac{\partial(\delta c_{V_o^{\cdot\cdot}})}{\partial y} \qquad \text{for } y=0 \quad (7)$$

From Eqs. (4), (5), (6) and (7), the electrode impedance $Z(\omega)$ is finally given as

$$Z(\omega) = R_{ch}\sqrt{\frac{1}{1+j\omega\ t_{ch}}} \quad (8)$$

$$\text{with } R_{ch} = \left(\frac{RT}{2F^2}\right)\sqrt{\frac{\tau}{(1-\varepsilon)c_{V_o^{\cdot\cdot}}D_{V_o^{\cdot\cdot}}A_s j_o}} \quad (9)$$

where $R_{ch}$ designates the characteristic resistance for the oxygen reduction reaction. According to Eq. (8), the ac-impedance spectrum exhibits a straight line inclined at a constant angle of 45° to the real axis at high frequencies, followed by an arc at low frequencies, which is frequently called the Gerischer behaviour [24].

The most remarkable point which should be mentioned here is that for the overall oxygen reduction involving oxygen vacancy diffusion through the electrode coupled with the electron exchange reaction at the electrode/gas interface, the two-dimensional electrochemical active region is not restricted to the TPBs, but it is significantly extended from the origin of the TPBs into the electrode/gas interface segments: $\lambda$ in Eq. (6) is usually taken as the extended active reaction length.

## Ac-impedance behaviour of the $(La_{0.85}Sr_{0.15})_{0.9}MnO_3$ electrode subjected to the preceding cathodic polarisation

In this work, to attain the mixed conducting state of $(La_{0.85}Sr_{0.15})_{0.9}MnO_3$, the electrode was previously subjected to the cathodic polarisation of −0.9 V at 1,273 K for 6 h. During the preceding cathodic polarisation, the partial reduction reaction of $Mn^{3+}$ to $Mn^{2+}$ at the electrode/electrolyte interface occurs simultaneously along with the oxygen reduction reaction at the TPBs, causing the formation of oxygen vacancies [17, 18]. The formation of oxygen vacancies is represented as follows:

$$\begin{aligned} &O_{O,LSM} + V_{O,YSZ}^{\cdot\cdot} + 2Mn_{LSM}^{3+} + 2e \\ &= V_{O,LSM}^{\cdot\cdot} + 2Mn_{LSM}^{2+} + O_{O,YSZ} \\ &\qquad (\text{Kröger} - \text{Vink notation}) \end{aligned} \quad (10)$$

$$|O_{O,YSZ}| + 2Mn_{LSM}^{3+} + 2e = |O_{O,LSM}| + 2Mn_{LSM}^{2+} \quad (11)$$

$$(\text{Schottky} - \text{Wagner notation})$$

The concentration of oxygen vacancies $c_{V_o^{\cdot\cdot}}$ generated during the prior cathodic polarisation is uniquely deter-

mined by the overpotential $\eta$ across the electrode/electrolyte interface [17, 21]:

$$c_{V_o^{\cdot\cdot}} = c^o_{V_o^{\cdot\cdot}} \exp\left(\frac{-2\alpha_2 F\eta}{RT}\right) \quad (12)$$

where $c^o_{V_o^{\cdot\cdot}}$ is the oxygen vacancy concentration in the as-sintered electrode without the preceding cathodic polarisation, and $\alpha_2$ is the transfer coefficient for the reduction reaction Eqs. (10) and (11). By taking the values of $c^o_{V_o^{\cdot\cdot}}$ and $\alpha_2$ as $5\times10^{-8}$ mol cm$^{-3}$ [23] and 0.5, respectively, the value of $c_{V_o^{\cdot\cdot}}$ was calculated from Eq. (12) to be $1.8\times10^{-4}$ mol cm$^{-3}$ at $T$=1,273 K.

The value of $c_{V_o^{\cdot\cdot}}$ obtained in this work is lower by more than one order of magnitude compared with $c_{V_o^{\cdot\cdot}}$ typically reported in the intrinsic mixed conductors, e.g. $La_{1-x}Sr_xCoO_3$ ($x$=0.2 and 0.4) [25]. Unfortunately, we failed to obtain the mixed conducting $(La_{0.85}Sr_{0.15})_{0.9}MnO_3$ electrode with the value of $c_{V_o^{\cdot\cdot}}$ higher than the critical concentration $8.5\times10^{-3}$ mol cm$^{-3}$ that was reported by Tagawa et al. [26], since the $(La_{0.85}Sr_{0.15})_{0.9}MnO_3$ electrode was observed to decompose into $La_2O_3$ and $Mn_3O_4$ phases when it was cathodically polarised below −0.9 V.

Figure 5a envisages the Nyquist plots of the ac-impedance spectrum, measured as a function of $T$ at $p_{O_2}$ =0.04 atm on the $(La_{0.85}Sr_{0.15})_{0.9}MnO_3$ electrode previously subjected to cathodic polarisation. Ac-impedance spectra theoretically calculated from Eq. (8) are also designated in Fig. 5a. In contrast to the case of the as-sintered electrode in Fig. 4a,b, the ac-impedance spectrum clearly displayed the Gerischer behaviour, as predicted from Eq. (8). As a matter of fact, the ac-impedance spectrum in Fig. 5a is quite similar in shape to those spectra determined from the intrinsically mixed conductors such as $La_{0.6}Sr_{0.4}CoO_3$ [25] and $(La_{0.6}Sr_{0.4})(Co_{0.2}Fe_{0.8})O_3$ [27]. This reflects that by the cathodic polarisation, the $(La_{0.85}Sr_{0.15})_{0.9}MnO_3$ electrode was altered to have the mixed electronic/ionic conducting property.

In view of the Gerischer impedance, consequently, it was recognised that the oxygen reduction reaction on the $(La_{0.85}Sr_{0.15})_{0.9}MnO_3$ electrode subjected to the preceding cathodic polarisation involves diffusion of oxygen vacancy through the electrode mixed with the electronic exchange reaction between oxygen vacancies and gaseous oxygen (charge transfer reaction) at the electrode/gas interface. The rate of the overall oxygen reduction is determined by the mixed control of the charge transfer reaction and the subsequent oxygen vacancy diffusion.

As a matter of fact, the Gerischer shape does not only reflect bulk diffusion mixed with the charge transfer reaction but also surface diffusion of oxygen molecules coupled with the adsorption reaction. If the Gerischer impedance resulted from the surface diffusion coupled with the adsorption reaction, it should be more dependent on the oxygen partial pressure than that of bulk diffusion coupled with the exchange reaction, because the kinetics of the

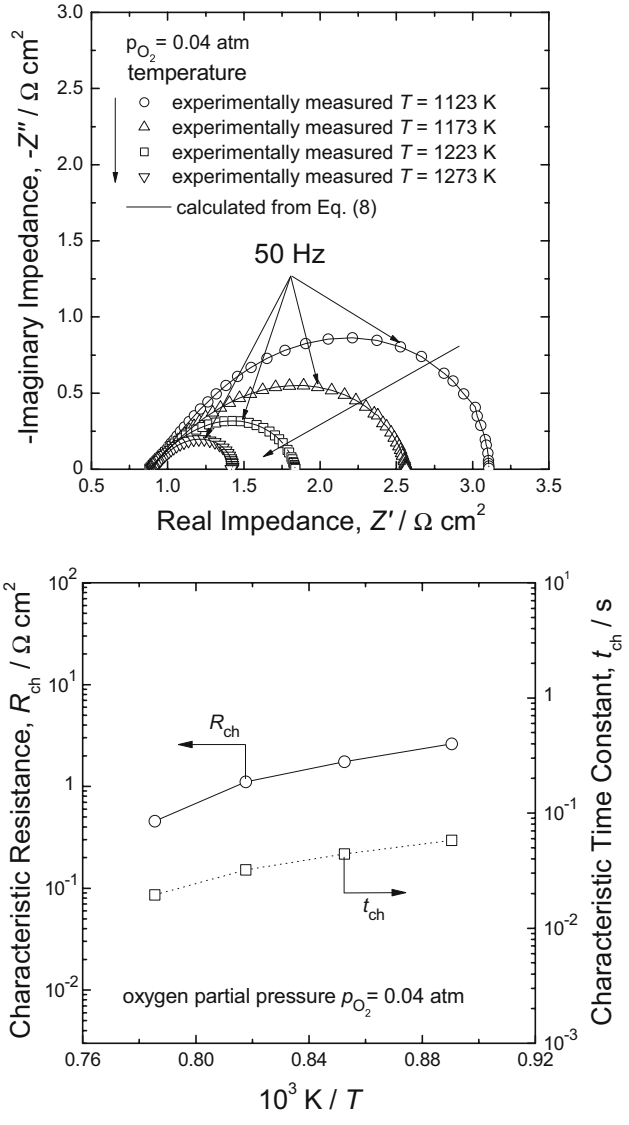


**Fig. 5** **a** Nyquist plots of the ac-impedance spectrum, ○, □, □ and □, experimentally obtained as a function of $T$ at $p_{O_2}$=0.04 atm from the as-sintered $(La_{0.85}Sr_{0.15})_{0.9}MnO_3$ electrode with $\varepsilon$=0.12 subjected to the preceding cathodic polarisation of −0.9 V for 6 h, (−) theoretically calculated from Eq. (8), and **b** the dependencies of the characteristic resistance $R_{ch}$ and the characteristic time constant $t_{ch}$ for oxygen reduction on the temperature, determined by fitting the measured impedance spectra to Eq. (8)

adsorption reaction is more influenced by $p_{O_2}$ as compared with that of the charge transfer reaction at the electrode surface. For most cases of surface diffusion on the LSM ($La_{0.8}Sr_{0.2}MnO_3$ and $La_{0.6}Sr_{0.4}MnO_3$) electrode, it was reported that the magnitude of the impedance arc is nearly dependent on $p_{O_2}^{-0.5}$ [10, 15, 28]. In the present work, however, the Gerischer impedance obtained from the $(La_{0.85}Sr_{0.15})_{0.9}MnO_3$ electrode depends in magnitude on $p_{O_2}^{-0.32}$. This indicates that the Gerischer impedance measured in this work is attributed to the bulk diffusion of oxygen vacancy through the $(La_{0.85}Sr_{0.15})_{0.9}MnO_3$ coupled with the charge transfer reaction.

In the present work, it was found that the ac-impedance spectrum measured on the $(La_{0.85}Sr_{0.15})_{0.9}MnO_3$ electrode held at 1,273 K for 72 h after the cathodic polarisation was exactly the same as the spectrum determined just after the cathodic polarisation, which justifies oxygen vacancies generated in the electrode during the prior cathodic polarisation are hardly annihilated during the ac-impedance measurement.

The measured impedance spectra in Fig. 5a were fitted to Eq. (8) to determine the characteristic resistance $R_{ch}$ and time constant $t_{ch}$ for oxygen reduction on the mixed conducting $(La_{0.85}Sr_{0.15})_{0.9}MnO_3$ electrode, and the resulting values are plotted on a logarithmic scale in Fig. 5b against the reciprocal of the absolute temperature (1/$T$).

Figure 6a,b depict the plots of the component diffusivity of oxygen vacancy $D_{V_O^{\cdot\cdot}}$ and of the equilibrium exchange flux $j_o$ versus the reciprocal of the absolute temperature (1/$T$), respectively, estimated from $t_{ch}$ in Eq. (5) and $R_{ch}$ in Eq. (9) at various values of $p_{O_2}$. When calculating $j_o$, we took the values of $W_{th}$ involved in Eq. (5) as 154 to 1,500, depending upon the values of $T$ and $p_{O_2}$ [29, 30]. The value of $D_{V_O^{\cdot\cdot}}$ was observed to linearly increase from approximately $2.0\times10^{-7}$ to approximately $5.5\times10^{-7}$ $cm^2$ $s^{-1}$ with decreasing (1/$T$), but it was almost independent of the value of $p_{O_2}$. On the other hand, $j_o$ gradually increased with rising $p_{O_2}$ over the whole $T$ range. Here, the value of $j_o$ was found to be lower by about one order of magnitude than $j_o$ evaluated from the $La_{1-x}Sr_xCoO_3$ ($x$=0.2 and 0.4) electrodes [25], which is ascribed to the lower concentration of oxygen vacancies in the $(La_{0.85}Sr_{0.15})_{0.9}MnO_3$ electrode.

As already pointed out in the preceding section "Theoretical consideration", the two-dimensional electrochemical active region for oxygen reduction involving oxygen vacancy diffusion coupled with the surface exchange reaction is extended from the origin of the TPBs into the electrode/gas interface segments. The length of the electrode/gas interface segments $\lambda$ calculated from Eq. (6) at various values of $p_{O_2}$ is plotted in Fig. 7 against the reciprocal of the absolute temperature (1/$T$), and the value of $\lambda$ ranged from 0.7 to 1.1 μm, depending upon $T$ and $p_{O_2}$. Since the increase of $j_o$ with $p_{O_2}$ dominated over the increase of $D_{V_O^{\cdot\cdot}}$ with $p_{O_2}$ as presented in Fig. 6a,b, the $\lambda$ term in Eq. (6) was determined to decrease with increasing $p_{O_2}$ over the whole $T$ range.

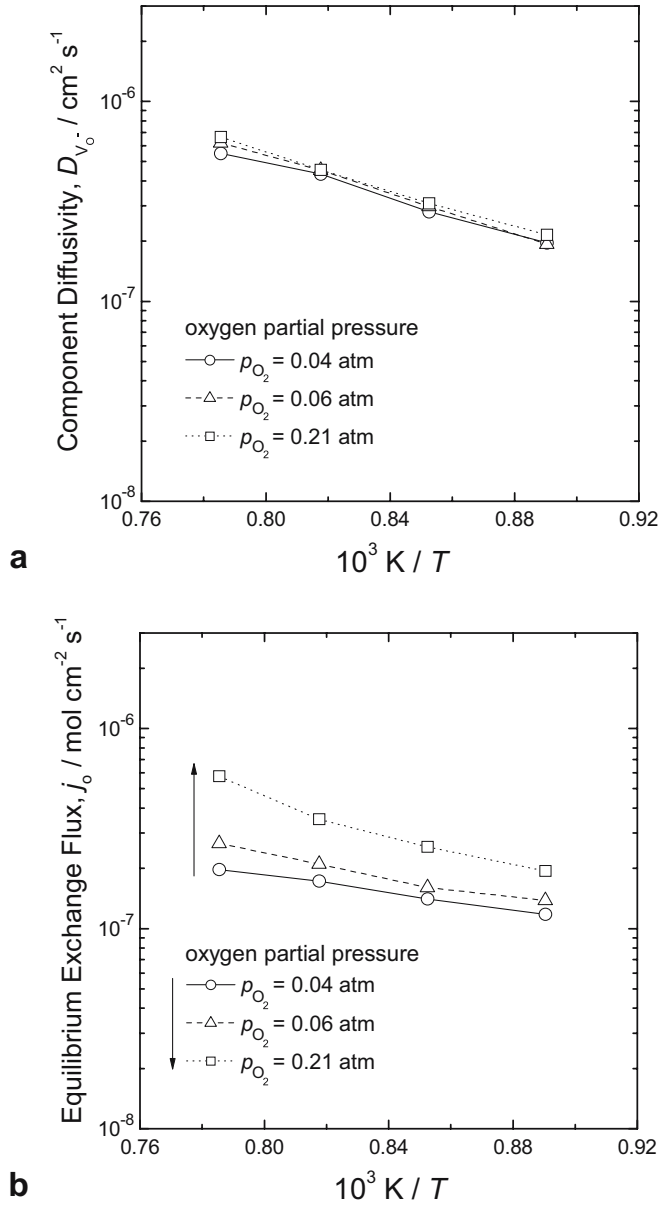


**Fig. 6** Plots of the component diffusivity of oxygen vacancy $D_{V_O^{\cdot\cdot}}$ **a** and the equilibrium exchange flux $j_o$ against the reciprocal of the absolute temperature (1/$T$) **b**, determined from the $(La_{0.85}Sr_{0.15})_{0.9}MnO_3$ electrode with $\varepsilon$=0.12 at various values of $p_{O_2}$. The electrode was previously subjected to the cathodic polarisation of −0.9 V for 6 h, and the values of $D_{V_O^{\cdot\cdot}}$ and $j_o$ were calculated from $R_{ch}$ and $t_{ch}$, respectively

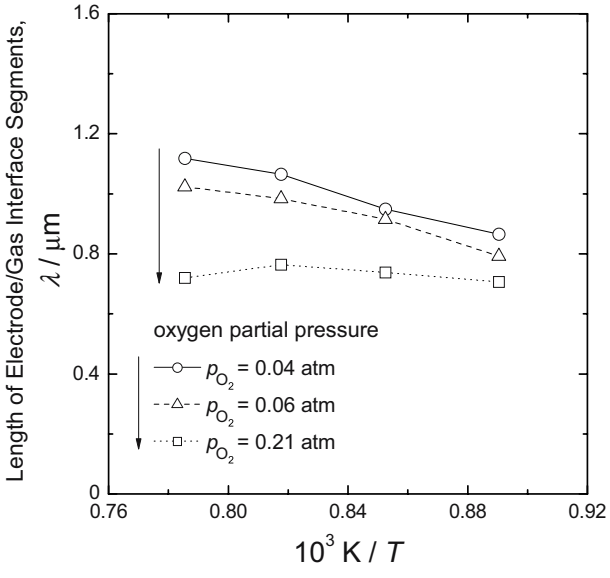


**Fig. 7** Plots of the length of the electrode/gas interface segments from the origin of TPBs $\lambda$ versus the reciprocal of the absolute temperature (1/$T$), obtained from the $(La_{0.85}Sr_{0.15})_{0.9}MnO_3$ electrode with $\varepsilon$=0.12 at various values of $p_{O_2}$. The electrode was previously subjected to the cathodic polarisation of −0.9 V for 6 h

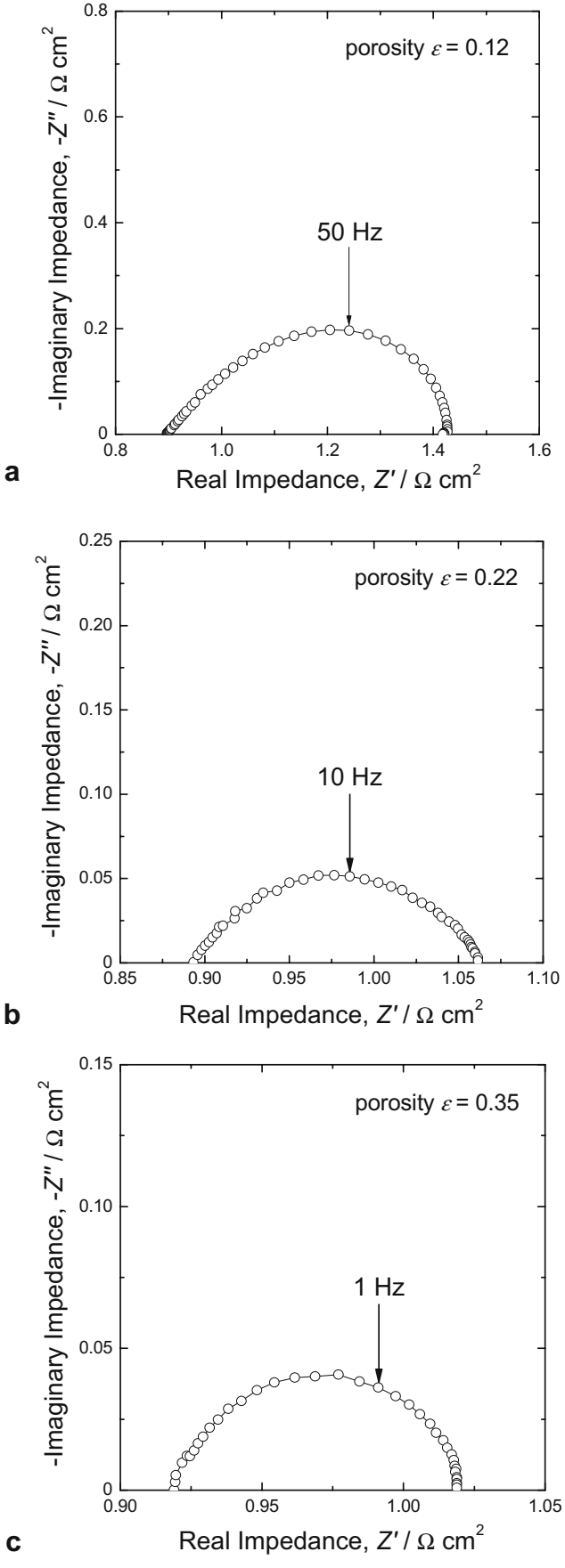


◀ **Fig. 8** Nyquist plots of the ac-impedance spectrum measured on the $(La_{0.85}Sr_{0.15})_{0.9}MnO_3$ electrodes with $\varepsilon$=0.12 **a**, $\varepsilon$=0.22 **b** and $\varepsilon$=0.35 **c** at $T$=1,273 K and $p_{O_2}$=0.04 atm. The electrode was previously subjected to the cathodic polarisation of −0.9 V for 6 h

Figure 8a–c illustrate the ac-impedance spectra in Nyquist representation, measured at $T$=1,273 K and $p_{O_2}$ = 0.04 atm on the $(La_{0.85}Sr_{0.15})_{0.9}MnO_3$ electrodes with different values of $\varepsilon$ which were previously subjected to the cathodic polarisation. As the $\varepsilon$ of the electrode increased, the measured impedance spectrum deviated more significantly from the Gerischer behaviour, finally to become one simple arc. Due to the fact that the TPB length $l_{TPB}$ increased with rising $\varepsilon$, it appears that the oxygen reduction reaction on the highly porous electrode proceeds under the condition that equilibrium for the charge transfer reaction is noticeably disturbed at the TPBs, and equilibrium for the subsequent diffusion of oxygen vacancy is practically undisturbed through the electrode. The value of $l_{TPB}$ is of great importance for the charge transfer-controlled oxygen reduction, whereas the value of $\lambda$ is valid for the mixed control of the charge transfer reaction and diffusion of oxygen vacancy. The following work would go into details with respect to the role of the electrode porosity in the oxygen reduction reaction on the mixed conducting electrode.

## Conclusions

In the present work, the oxygen reduction reaction on the porous $(La_{0.85}Sr_{0.15})_{0.9}MnO_3$ electrode with mixed conducting property was examined by means of analysis of the ac-impedance spectra. The results are summarised as follows:

1. The Nyquist plot of the ac-impedance spectrum obtained from the as-sintered $(La_{0.85}Sr_{0.15})_{0.9}MnO_3$ electrode showed two depressed arcs which are associated with the charge transfer at the TPBs in the high-frequency range and diffusion of adsorbed oxygen along the electrode surface in the low-frequency range, respectively.
2. The ac-impedance spectrum measured on the as-sintered $(La_{0.85}Sr_{0.15})_{0.9}MnO_3$ electrode subjected to the preceding cathodic polarisation clearly exhibited the Gerischer behaviour. This reflects that the overall oxygen reduction reaction on the mixed conducting electrode proceeds under the condition where diffusion of oxygen vacancy in the electrode is kinetically coupled with the electron exchange reaction between oxygen vacancies and gaseous oxygen (charge transfer reaction) at the electrode/gas interface.
3. According to the theoretical impedance model based on the Gerischer behaviour, it is suggested that the two-dimensional electrochemical active region for oxygen reduction extends from the origin of TPBs to the electrode/gas interface segments. The length of the electrode/gas interface segments from the origin of

TPBs, $\lambda$, was calculated to be approximately 0.7 to 1.1 μm on average below the electrode porosity $\varepsilon$ 0.12.

4. As the electrode porosity increased, the ac-impedance spectrum deviated more significantly from the Gerischer behaviour, which suggests that due to the increased TPB extent $l_{TPB}$, the overall oxygen reduction reaction on the highly porous electrode proceeds mainly by the charge transfer reaction at the TPBs for which the equilibria are strongly impeded. The subsequent oxygen vacancy diffusion occurs undisturbedly through the electrode.

**Acknowledgements** The receipt of a research grant No. N-FC12-P-03-3-010 for the 5-year period 2004–2009 from Korea Energy Management Corporation is gratefully acknowledged. Furthermore, this work was partly supported by the Brain Korea 21 project.

## References

1. Stambouli AB, Traversa E (2002) Renew. Sust Energ Rev 6:433
2. Ormerod RM (2003) Chem Soc Rev 32:17
3. Minh NQ, Badwal SPS, Bannister MJ, Hannink RHJ (ed) (1993) Science and technology of zirconia. Technomic, Lancaster, pp 652–687
4. Minh NQ, Takahashi T (1995) Science and technology of ceramic fuel cells. Elsevier, Amsterdam, pp 117–146
5. Vielstich W, Gasteiger HA, Lamm A (2003) Handbook of fuel cells—fundamentals, technology and applications. Wiley, New York, pp 588–600
6. Mizusaki J, Amano K, Yamauchi S, Fueki K (1987) Solid State Ionics 22:313
7. Østergard MJL, Mogensen M (1993) Electrochim Acta 38:2015
8. Hammouche A, Siebert E, Hammou A, Kleitz M (1994) J Electrochem Soc 141:2118
9. Gharbage B, Pagnier T, Hammou A (1994) Solid State Ionics 72:248
10. Siebert E, Hammouche A, Kleitz M (1995) Electrochim Acta 40:1741
11. Yokokawa H, Horita T, Sakai N, Dokiya M, Kawada T (1996) Solid State Ionics 86–88:1161
12. Heuveln FHV, Bouwmeester HJM (1997) J Electrochem Soc 144:134
13. Ioroi T, Hara T, Uchimoto Y, Ogumi Z, Takehara ZI (1998) J Electrochem Soc 145:1999
14. Jiang SP, Love JG, Zhang JP, Hoang M, Ramprakash Y, Hughes AE, Badwal SPS (1999) Solid State Ionics 121:1
15. Matsuzaki Y, Yasuda I (1999) Solid State Ionics 126:307
16. Nowotny J, Rekas M (1998) J Am Ceram Soc 81:67
17. Jiang Y, Wang S, Zhang Y, Yan J, Li W (1998) J Electrochem Soc 145:373
18. Chen XJ, Khor KA, Chan SH (2003) J Power Sources 123:17
19. Adler SB, Lane JA, Steele BCH (1996) J Electrochem Soc 143:3554
20. Satterfield CN, Sherwood TK (1963) The role of diffusion in catalysis. Addison-Wesley, Boston, pp 11–28
21. Kuznecov M, Otschik P, Obenaus P, Eichler K, Schaffrath W (2003) Solid State Ionics 157:371
22. Carter S, Selcuk A, Chater RJ, Kajda J, Kilner JA, Steele BCH (1992) Solid State Ionics 53–56:597
23. Yasuda I, Ogasawara K, Hishinuma M, Kawada T, Dokiya M (1996) Solid State Ionics 86–88:1197
24. Boukamp BA, Bouwmeester HJM (2003) Solid State Ionics 157:29
25. Adler SB (1998) Solid State Ionics 111:125
26. Tagawa H, Mori N, Takai H, Yonemura Y, Minamiue H, Inaba H, Mizusaki J, Hashimoto T (1997) Proc. of the 5th Int. Symp. on SOFC, vol PV 97–40, pp 785
27. Jiang SP (2002) Solid State Ionics 146:1
28. Tsuneyoshi K, Mori K, Sawata A, Mizusaki J, Tagawa H (1989) Solid State Ionics 35:263
29. Belzner A, Gur TM, Huggins RA (1992) Solid State Ionics 57:327
30. de Souza RA, Kilner JA (1998) Solid State Ionics 106:175